Brueckner-Hartree-Fock calculations for finite nuclei with renormalized realistic forces

B. S. Hu (胡柏山), F. R. Xu (许甫荣), Q. Wu (吴强), Y. Z. Ma (马远卓), and Z. H. Sun (孙中浩)

Phys. Rev. C **95**, 034321 — Published 27 March 2017

DOI: 10.1103/PhysRevC.95.034321

Brueckner-Hartree-Fock calculations for finite nuclei with renormalized realistic forces

B. S. Hu (胡柏山), F. R. Xu (许甫荣),* Q. Wu (吴强), Y. Z. Ma (马远卓), and Z. H. Sun (孙中浩)

School of Physics, and State Key Laboratory of Nuclear Physics and Technology, Peking University, Beijing 100871, China

(Dated: March 5, 2017)

Abstract

One can adopt two-step G-matrix approximations for the Brueckner-Hartree-Fock (BHF) calculations. The first G-matrix is to soften the bare force, and the second one is to include the high-order correlations of the interaction in medium. The first G-matrix calculation for two-nucleon interaction should be done in the center-of-mass coordinate. As another alternative BHF approach, we have adopted the $V_{\text{low-}k}$ technique to soften the interaction and used the G-matrix to include high-order correlations. The $V_{\text{low-}k}$ renormalization leads to high-momentum and low-momentum components of the interaction decoupled. With the $V_{\text{low-}k}$ potential, we have performed the BHF calculations for finite nuclei. The G-matrix elements with exact Pauli exclusions are calculated in the self-consistent BHF basis. To see effects from further possible correlations beyond BHF, we have simultaneously performed renormalized BHF (RBHF) calculations with the same potential. In RBHF, the mean field derived from realistic forces is modified by introducing the particle-occupation depletion resulting from many-body correlations. The ground-state energies and radii of the closed-shell nuclei, ^{4}He, ^{16}O and ^{40}Ca, have been investigated. The convergences of the BHF and RBHF calculations have been discussed, and compared with other *ab-initio* calculations with the same potential.

PACS numbers: 21.60.De, 21.30.Fe, 21.10.Dr, 21.10.Ft

* frxu@pku.edu.cn

I. INTRODUCTION

One of current fundamental goals in nuclear theory is to use realistic nuclear forces for nuclear structure calculations. Realistic nucleon-nucleon (NN) interaction provides the high-quality descriptions of the NN scattering phase shifts and deuteron properties. The Hartree-Fock (HF) method is one of widely used approaches for solving many-body quantum systems, with approximating the wavefunction by a single Slater determinant based on single-particle states. The single-particle states are the eigenstates of the one-body HF potential U which can be derived from the two-body NN interaction V by $U = \mathrm{Tr}(V\rho)$ with ρ being density [1]. The conventional HF method describes the motions of nucleons in the average field of other nucleons and neglects higher-order correlations, while the higher-order correlations are important for calculations starting from realistic nuclear forces [2–4].

The Brueckner-Hartree-Fock (BHF) theory gives an improved definition of one-body potential U by replacing the two-body interaction V with the so-called reaction G-matrix which sums up ladder diagrams to infinite orders and gives an effective two-body interaction allowing for many-body correlations [5]. In the BHF theory, the important diagrams in perturbation expansion are summed by introducing the G-matrix operator. The Renormalized Brueckner-Hartree-Fock (RBHF) approach [6–9] makes further modification to the BHF average field U, which takes into account the depletions of occupied single-particle states due to many-body correlations. The depletion mechanism cancels a large class of additional diagrams (called saturation-potential diagrams or rearrangement diagrams) in calculating the ground-state energy and single-particle energies, e.g., the typical diagram shown in Fig. 1.

Realistic interactions, such as CD-Bonn [10], Nijmegen [11], Argonne v_{18} [12], INOY [13], and chiral potential [14, 15], exhibit strong short-range correlations or high-momentum components which cause nonconvergence problem in nuclear structure calculations. The problem is more serious for these potentials that have a so-called hard core [5]. The matrix elements of a hard core potential, $\langle\phi(r)|V_{NN}|\phi(r)\rangle$, in uncorrelated two-body wave function $\phi(r)$ can become extremely large or even divergent since the uncorrelated wave function can be non-zero at the distance smaller than the hard-core radius.

A traditional approach to deal with the strong short-range correlations is the G-matrix renormalization in the Brueckner-Bethe-Goldstone theory [16–18]. By allowing nucleons to be scattered to intermediate states above the HF Fermi surface, the G-matrix potential

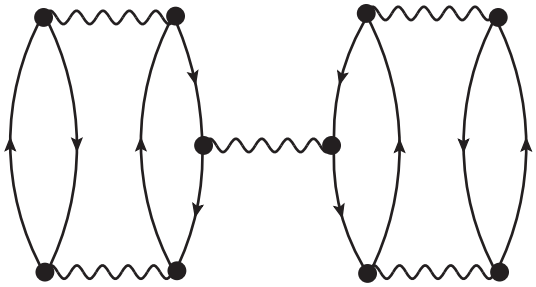

FIG. 1. The typical diagram cancelled in the RBHF method by including occupation probabilities in the definition of the single-particle potential U.

includes high-order correlations which are missing in the HF approximation. On the other hand, the G-matrix operator contains a denominator with the energy difference between scattered and initial states, which leads to a weakening effect on the coupling between the low-momentum and high-momentum components of the force, and thus softens the interaction. In practical calculations, usually two steps of the G-matrix approximation are performed [5, 18–21]. First, in the center-of-mass coordinate, a reference G-matrix is calculated with the approximate Pauli exclusion. This step is mainly to soften the force. With the softened reference G-matrix potential, the second step of the G-matrix calculations is performed in the laboratory coordinate. This step is mainly to include the high-order correlations. Such two-step G-matrix approximation can expedite the convergence of many-body calculations [5].

In the present work, we use the $V_{\text{low-}k}$ technique to soften the bare force. The $V_{\text{low-}k}$ renormalization integrates out high-momentum components of the force [22, 23]. The effective interaction $V_{\text{low-}k}$ preserves the low-energy physics of the realistic force (e.g., low-energy phase shifts) and is both energy and mass independent [22, 23]. With the $V_{\text{low-}k}$ renormalized interaction, we perform the BHF and RBHF calculations for finite nuclei with one-step G-matrix approximation which is to include the high-order correlations (or called in-medium effects). The BHF calculation based on the $V_{\text{low-}k}$ potential has been suggested by Kuckei *et al.* in Ref. [24], where the long-range correlations from configurations inside their model space are treated within the framework of the Green's function approach.

II. THEORETICAL FRAMEWORK

A. The effective Hamiltonian

The intrinsic Hamiltonian of the A-nucleon system used in this paper reads

$$\begin{aligned}\hat{\mathrm{H}} &= \sum_{i=1}^{A}\left(1-\frac{1}{A}\right)\frac{\vec{p}_i^{\,2}}{2m}+\sum_{i<j=1}^{A}\left(\hat{V}_{ij}^{(2)}-\frac{\vec{p}_i\cdot\vec{p}_j}{mA}\right)\\ &= \sum_{i=1}^{A}\hat{T}_i+\sum_{i<j=1}^{A}\hat{V}_{ij},\end{aligned} \tag{1}$$

where $\hat{V}^{(2)}=\hat{V}_{NN}+\hat{V}_{\mathrm{Coul}}$ with $\hat{V}_{NN}$ being the NN interaction and $\hat{V}_{\mathrm{Coul}}$ being the coulomb interaction. We do not include three-body interaction. In the present work, the $\hat{V}_{NN}$ is derived from Argonne v_{18} potential [12] by using the $V_{\text{low-}k}$ technique. The $V_{\text{low-}k}$ method is a renormalization group approach and is used to soften the short-range repulsion and short-range tensor components of the initial interaction. It integrates out the high-momentum components of the nuclear force in the momentum space while preserves accurately the low-momentum physics of the force. This process leads to the decoupling between low-momentum and high-momentum parts of the Hamiltonian. The renormalized potential becomes softer and more perturbative than the initial force. We used the $V_{\text{low-}k}$ renormalization with the Lee-Suzuki projection [23, 25].

B. Brueckner-Hartree-Fock Theory

The BHF approach has almost the same formalism as the HF approximation except the mean field U which is produced by using the G-matrix in BHF. The G-matrix potential is obtained by the Bethe-Goldstone equation,

$$G(\omega)=V+V\frac{Q}{e}G(\omega), \tag{2}$$

with the energy denominator $e=\omega-h_0(1)-h_0(2)+i\eta$. ω is the starting energy, and $h_0(i)$ ($i=1,2$ for particle 1 and 2, respectively) is the single-particle Hamiltonian with the one-body mean field U. The Pauli exclusion operator Q forbids the two interacting nucleons scattered into the states occupied already by other nucleons. The Pauli exclusion operator Q should be defined in the self-consistent BHF basis. Practical calculations usually take

two-step G-matrix approximations. First, a reference G-matrix is calculated by [5]

$$G_0 = V_{NN} + V_{NN}\frac{Q_0}{e_0}G_0, \tag{3}$$

using the approximate Pauli operator Q_0 and energy denominator e_0 relative to the "true" reaction matrix G [5]. G_0 is calculated in the center-of-mass coordinate, which is to deal with short-range correlations. There are different methods to approximate the reference G_0 in the history of the BHF development. A typical G_0 calculation is called the angle-averaged Pauli operator approximation [5, 20]. The second typical method is Eden and Emery approximation [21] in which the Pauli operator is diagonalized in the center-of-mass representation. There is another G_0 approximation called the reference-spectrum method [19] in which one simply sets $Q_0 = 1$ for the reference G_0 calculation. After getting G_0, the "true" G is calculated by using the Bethe-Brandow-Petschek (BBP) identity [18]

$$G = G_0 + G_0\left(\frac{Q}{e} - \frac{Q_0}{e_0}\right)G. \tag{4}$$

In most cases, people do not use a self-consistent Pauli exclusion operator in G-matrix calculations, while they correct G_0 in a harmonic oscillator (HO) representation. This means that the occupation or unoccupation of the orbit is determined in the HO basis rather than in the BHF basis. In the present work, we define the Pauli exclusion operator in the BHF basis. Due to the inclusion of high-order perturbation terms (high-order correlations), the G-matrix potential is beyond the conventional HF mean field. The important diagrams include not only the ladder diagrams to infinite orders, but also some diagrams that are included in hole-hole and particle-hole G-matrix bubble insertions by putting G-matrix on the energy shell (see Fig. 2 as an example) or in particle-particle bubble insertions by the off-shell prescription. Here "on-energy-shell" means that ω in Eq. (2) is equal either to the energy of the initial two-particle state or to the energy of the final two-particle state. Off-energy-shell (or simply called off-shell) G-matrix elements are calculated without the equal energies of initial and final states. The hole-hole and particle-hole bubble insertions can be cancelled by constructing an appropriate mean field U [26]. For example, in Fig. 3 the diagrams in the lower panel cancel those in the upper panel. Figure 4 gives the Brueckner-Goldstone expansion for the ground-state energy, where V is replaced by G in the perturbation expansion [27] and ladder diagrams are omitted. We can see that the bubble insertions can be cancelled by choosing U [26].

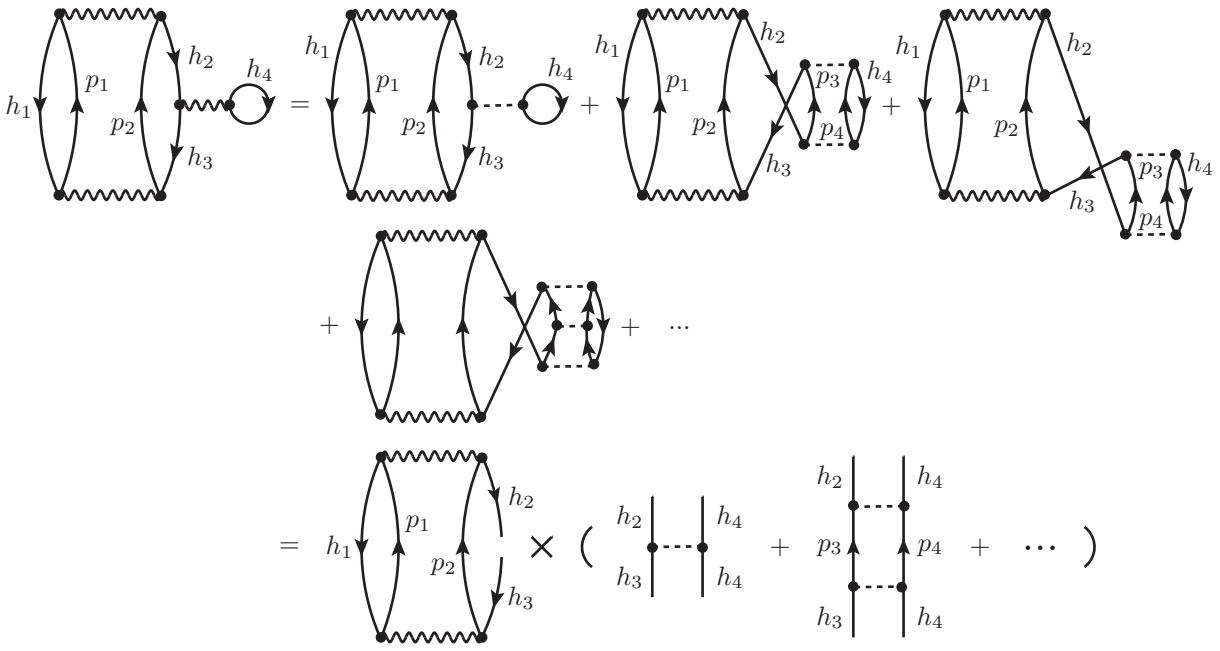

FIG. 2. An example of the diagrams which can be included in hole-hole G-matrix bubble insertions by putting G-matrix on the energy shell.

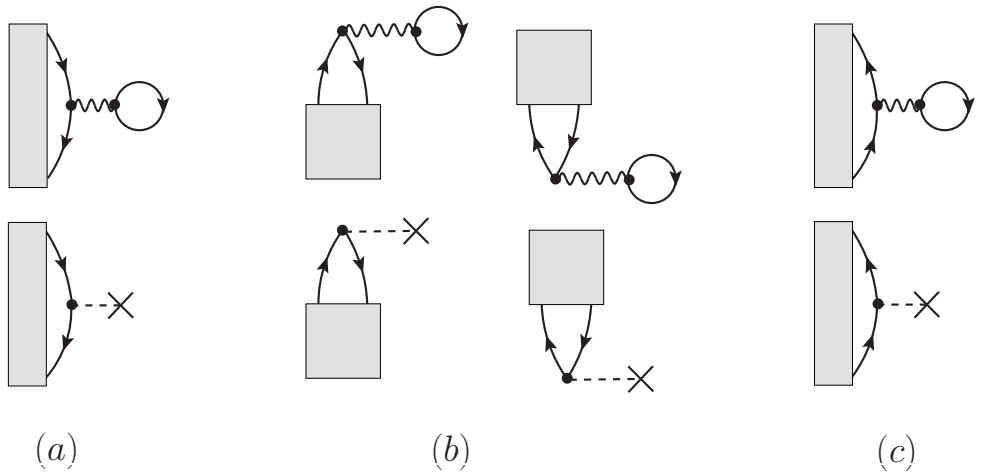

FIG. 3. Examples of diagrams included in the BHF calculation. The wavy line signifies the G-matrix interaction, while the dashed line terminated by a cross signifies the single-particle potential U.

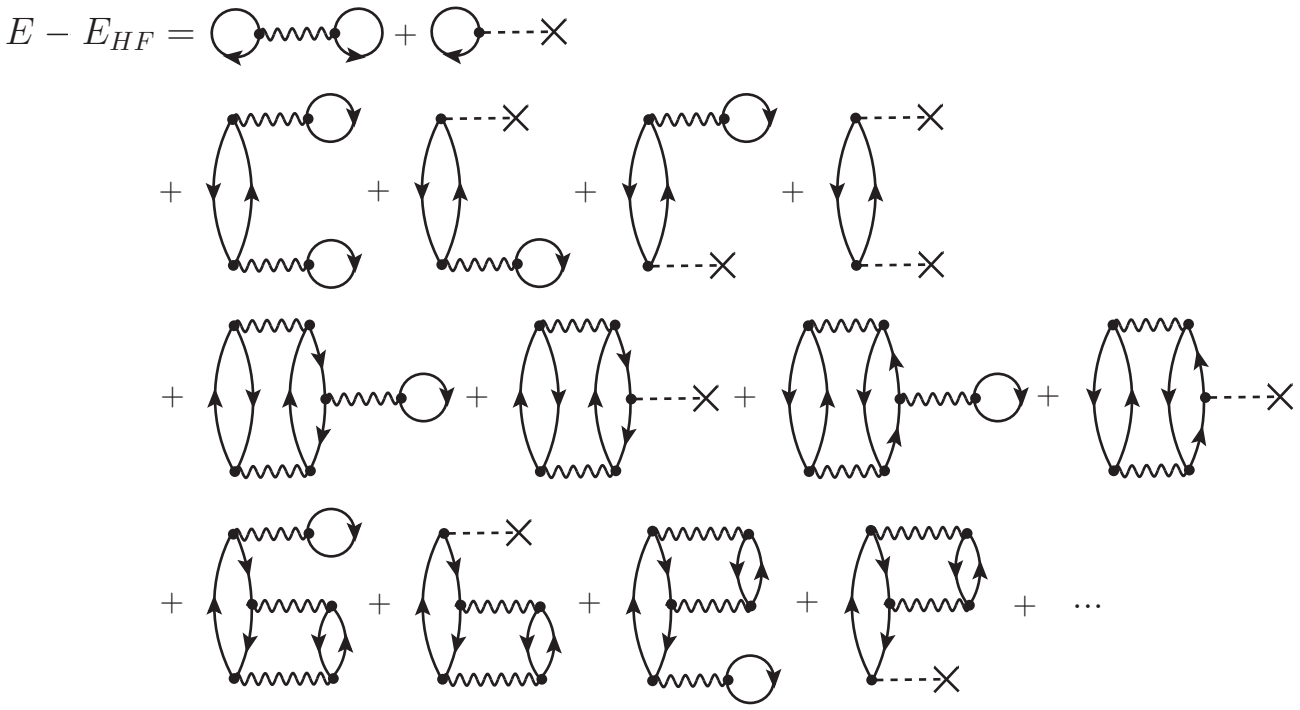

FIG. 4. The first-, second-, and some third-order anti-symmetrized Goldstone diagrams of energy corrections in the Brueckner-Goldstone expansion [26]. The wavy line signifies G-matrix interaction, while dashed line terminated by a cross signifies the single-particle potential U.

A conventional choice for the matrix elements of the BHF potential U [26, 28] is

$$\langle a|U|b\rangle = \begin{cases} \frac{1}{2}\sum\limits_{h\le\varepsilon_{\rm F}} \langle ah|G(\varepsilon_a+\varepsilon_h)+G(\varepsilon_b+\varepsilon_h)|bh\rangle & \text{for } a,b\le\varepsilon_{\rm F} \\ \sum\limits_{h\le\varepsilon_{\rm F}} \langle ah|G(\varepsilon_a+\varepsilon_h))|bh\rangle & \text{for } a\le\varepsilon_{\rm F}, b>\varepsilon_{\rm F} \\ \sum\limits_{h\le\varepsilon_{\rm F}} \langle ah|G(\varepsilon_b+\varepsilon_h))|bh\rangle & \text{for } a>\varepsilon_{\rm F}, b\le\varepsilon_{\rm F} \\ \frac{1}{2}\sum\limits_{h\le\varepsilon_{\rm F}} \langle ah|G(\bar{\varepsilon}_a+\varepsilon_h)+G(\bar{\varepsilon}_b+\varepsilon_h)|bh\rangle & \text{for } a,b>\varepsilon_{\rm F} \end{cases}, \qquad (5)$$

where the letter h indicates an occupied single-particle orbit (i.e., a hole state) in the BHF basis, p stands for an empty level (i.e., a particle state) and a, b, ... label any states (either hole or particle). $\varepsilon_{\rm F}$ is the Fermi energy, and $\bar{\varepsilon}_a = 2\varepsilon_0 - \varepsilon_a$ with ε_0 being the average energy of the occupied single-particle states. For the U elements involving hole states, i.e., $\langle h|U|a\rangle$, the on-energy-shell definition of the $G(\omega)$-matrix guarantees the exact cancellations of hole-hole and particle-hole diagrams with bubble insertions, according to the BBP theorem [18]. The ω definition for a particle-particle element $\langle p_1|U|p_2\rangle$ is a somewhat controversial matter. The

particle-particle elements are intended to cancel the corresponding off-shell particle-bubble diagrams. Since $\langle p_1|U|p_2\rangle$ depends on the excitation energy of remainder diagrams, a self-consistent treatment of particle-bubble diagrams is complicated. It has been found that the total contribution from all three-body cluster diagrams to the energy of nuclear matter is much smaller than the contribution from single-particle bubble diagrams [29]. Therefore, if one wants particle-particle elements to cancel the three-body cluster diagrams, the particle-particle elements should not be very large. In the previous works [1, 5, 26], the $\langle p_1|U|p_2\rangle$ elements are set to be zero. We have tested both calculations with the prescription given by Eq. (5) or setting $\langle p_1|U|p_2\rangle = 0$.

In the present work, we limit the BHF calculations to closed-shell spherical nuclei. The spherical symmetry preserves the quantum numbers of the orbital angular momentum (l), the total angular momentum (j) and its projection (m_j). In the spherical closed shell, the BHF single-particle eigenvalues are independent of the magnetic quantum number m_j, which leads to a $2j+1$ degeneracy. We calculate the $G(\omega)$ elements in the angular momentum coupled scheme. The BHF single-particle states are denoted by $|a\rangle = |\nu l j m_t\rangle$ with m_t for the isospin projection and ν for other quantum numbers. We define an anti-symmetrized two-particle state with good angular momentum J and projection M,

$$|(ab)JM\rangle = \frac{1}{\sqrt{(1+\delta_{ab})}} \sum_{m_a,m_b} \langle j_a m_a j_b m_b|JM\rangle |(am_a)(bm_b)\rangle. \tag{6}$$

The G-matrix elements which are needed for the calculation of the BHF potential can be written as

$$\begin{aligned}\langle (ab)JM|G(\varepsilon_a^{'}+\varepsilon_b^{'})|(cd)JM\rangle =& \langle (ab)JM|\hat{V}|(cd)JM\rangle \\ &+\frac{1}{2}\sum_{r,s>\varepsilon_{\rm F}} \langle (ab)JM|\hat{V}|(rs)JM\rangle \\ &\times \frac{1+\delta_{rs}}{\varepsilon_a^{'}+\varepsilon_b^{'}-\varepsilon_r-\varepsilon_s} \langle (rs)JM|G(\varepsilon_a^{'}+\varepsilon_b^{'})|(cd)JM\rangle, \end{aligned} \tag{7}$$

with

$$\varepsilon_a^{'} = \begin{cases} \varepsilon_a & \text{for } a \le \varepsilon_{\rm F} \\ 2\varepsilon_0 - \varepsilon_a & \text{for } a > \varepsilon_{\rm F} \end{cases}. \tag{8}$$

We solve Eq. (7) by using matrix inversion method [26].

With the G-matrix elements obtained thus, the potential U can be calculated by Eq. (5). Then we can obtain single-particle energies ε_a and wavefunctions $|a\rangle$ by iterating the BHF

equation [1],

$$\langle a|\hat{H}_0|b\rangle = \langle a|(\hat{T}+U)|b\rangle = \varepsilon_a \delta_{ab}. \tag{9}$$

The practical BHF calculation is complicated. In the present work, we first use the Woods-Saxon (WS) basis to obtain initial G-matrix elements by solving Eq. (7), and then calculate initial U-potential elements by using Eq. (5) in the WS basis. With the initial potential, we diagonalize the BHF equation (i.e., Eq. (9)) which gives the initial BHF basis. In the BHF basis, we recalculate the G-matrix and U-potential elements, and diagonalize the BHF equation again. Such iteration is repeated in the BHF basis until the convergence is achieved. This process is similar to the solution of spherical HF as shown in Ref. [30]. The bulk properties of finite nuclei can be calculated within the HF framework. For example, the ground-state energy is given by

$$\begin{aligned} E_{\rm BHF} &= \sum_{h_1=1}^{A} \langle h_1|\hat{T}|h_1\rangle + \frac{1}{2}\sum_{h_1,h_2=1}^{A} \langle h_1 h_2|G(\varepsilon_{h_1}+\varepsilon_{h_2})|h_1 h_2\rangle \\ &= \sum_{h_1=1}^{A} \varepsilon_{h_1} - \frac{1}{2}\sum_{h_1,h_2=1}^{A} \langle h_1 h_2|G(\varepsilon_{h_1}+\varepsilon_{h_2})|h_1 h_2\rangle. \end{aligned} \tag{10}$$

C. Renormalized Brueckner-Hartree-Fock Theory

For comparison, we have also performed the RBHF calculations for finite nuclei. The RBHF approach modifies the BHF potential by taking into account the single-particle occupation depletion resulting from two-body correlations. In detail, it introduces an occupation probability which is less than 1 for a occupied single-particle orbit bellow the HF Fermi surface, correspondingly introduces occupation-probability diagrams (or called saturation-potential diagrams or rearrangement diagrams). The occupation probability is defined by

$$P_{h_1} = \left[1 - \sum_{h_2}\langle h_1 h_2|\frac{\partial G(\omega)}{\partial \omega}|h_1 h_2\rangle P_{h_2}\right]^{-1}_{\omega=\epsilon_{h_1}+\epsilon_{h_2}}, \tag{11}$$

where the renormalized single-particle energy is

$$\epsilon_{h_1} = \langle h_1|T|h_1\rangle + \sum_{h_2}\langle h_1 h_2|G(\omega=\epsilon_{h_1}+\epsilon_{h_2})|h_1 h_2\rangle P_{h_2}. \tag{12}$$

With Eqs. (2) and (11), we have [31],

$$\frac{\partial G(\omega)}{\partial \omega} = -G(\omega)\left(\frac{Q}{\omega - H_0(1) - H_0(2)}\right)^2 G(\omega), \tag{13}$$

and

$$P_{h_1} = \left[1 + \sum_{h_2 p_1 p_2} \frac{1}{2} \left(\frac{\langle h_1 h_2 | G(\omega = \epsilon_{h_1} + \epsilon_{h_2}) | p_1 p_2 \rangle}{\epsilon_{h_1} + \epsilon_{h_2} - \epsilon_{p_1} - \epsilon_{p_2}} \right)^2 P_{h_2} \right]^{-1}. \tag{14}$$

We use the self-consistent iteration procedure to solve the above occupation probability.

The ground-state energy in the RBHF theory is

$$\begin{aligned} E_{\rm RBHF} =& \sum_{h_1} \langle h_1 | T | h_1 \rangle + \frac{1}{2} \sum_{h_1, h_2} \langle h_1 h_2 | G(\epsilon_{h_1} + \epsilon_{h_2}) | h_1 h_2 \rangle P_{h_1} P_{h_2} \\ &+ \sum_{h_1, h_2} (1 - P_{h_1}) \langle h_1 h_2 | G(\epsilon_{h_1} + \epsilon_{h_2}) | h_1 h_2 \rangle P_{h_2}. \end{aligned} \tag{15}$$

The last term is the "over-counting correction" which should be included in the total energy, since single-particle energies are renormalized with occupation probabilities [31–33].

III. CALCULATIONS AND DISCUSSIONS

We have performed the BHF and RBHF calculations for closed-shell nuclei, ^{4}He, ^{16}O and ^{40}Ca, and benchmarked with other *ab-initio* calculations. The $V_{\text{low-}k}$ effective interaction derived from Argonne v_{18} potential [12] is adopted. A $V_{\text{low-}k}$ cutoff $\Lambda = 1.9$ fm^{-1} is taken for the ^{4}He calculation to compare with the existing Faddeev-Yakubovsky (FY) [34, 35] and coupled-cluster (CC) results. For ^{16}O and ^{40}Ca, we take $\Lambda = 2.1$ fm^{-1} to compare with the existing calculations of the CC [35] and importance-truncated NCSM (IT-NCSM) [36]. In our calculations, the self-consistent BHF (or RBHF) basis is expanded in the HO basis. The HO basis is truncated by a cutoff according to the shell number $N_{\rm shell} = \text{Max}(2n + l + 1)$ where the labels are standard with n and l for the radial and orbital angular momentum quantum numbers of the HO basis, respectively. $N_{\rm shell}$ indicates how many major HO shells are included in the truncation.

Figure 5 shows the ^{4}He, ^{16}O and ^{40}Ca ground-state energies calculated by BHF and RBHF as a function of the oscillator parameter $\hbar\Omega$ with different $N_{\rm shell}$. The BHF single-particle potential U is calculated by Eq. (5). The G-matrix elements given by Eq. (7) are obtained by the matrix inversion method. We see that both BHF and RBHF give calculations almost independent on the oscillator parameter $\hbar\Omega$ at $\hbar\Omega \geq$18 MeV. For example, in the BHF calculations at $\hbar\Omega$=22 MeV, the ^{40}Ca ground-state energy with $N_{\rm shell}$=11 is -551.5 MeV, while it is -552.1 MeV with $N_{\rm shell}$=12, showing the convergence of the present calculations

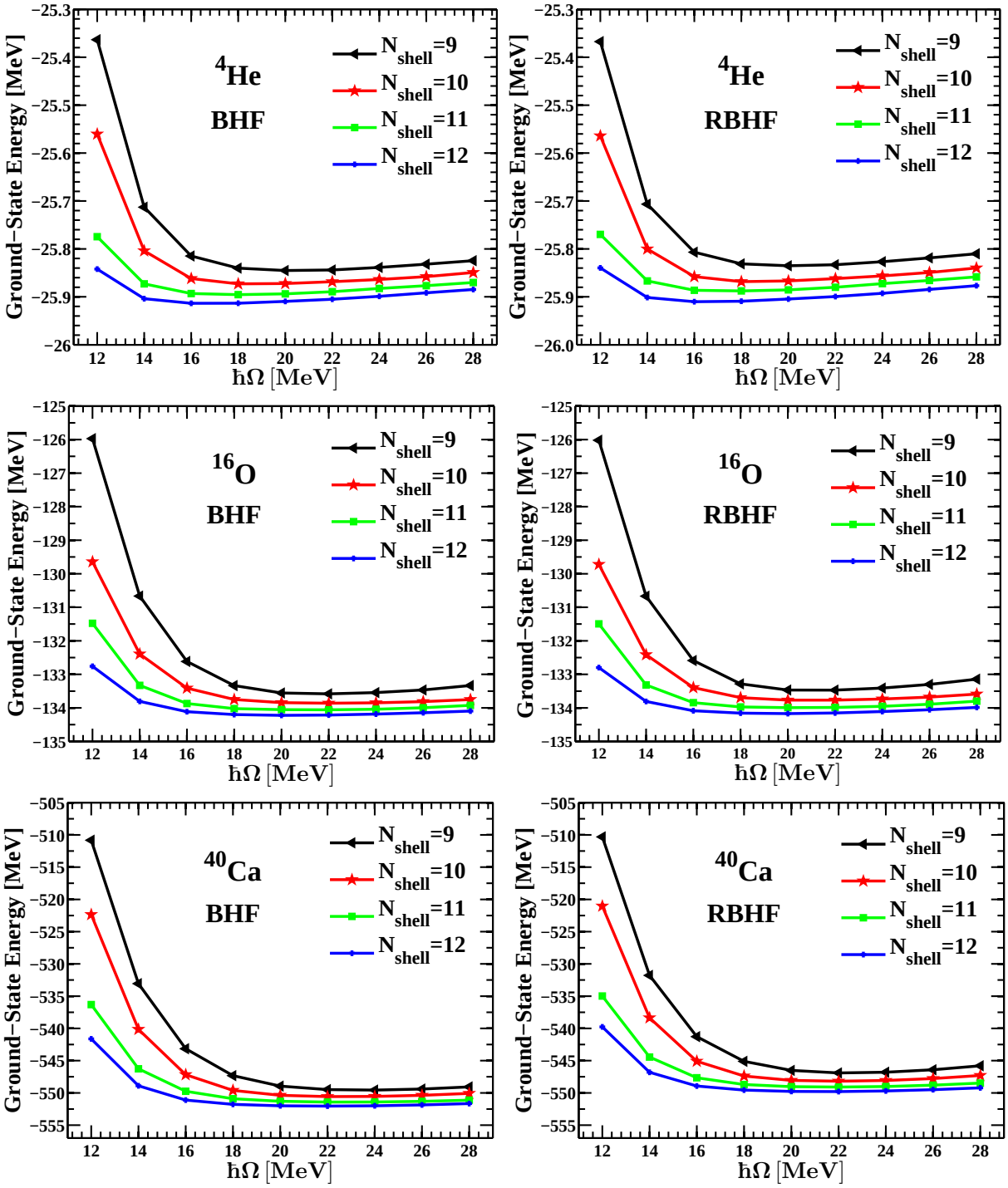

FIG. 5. The BHF and RBHF calculations for ^{4}He, ^{16}O and ^{40}Ca as a function of the oscillator parameter $\hbar\Omega$ with the $V_{\text{low-}k}$ effective interaction derived from the Argonne v_{18} potential [12] at cutoff momenta Λ=1.9 fm^{-1} for ^{4}He and Λ=2.1 fm^{-1} for ^{16}O and ^{40}Ca, respectively. Such cutoffs were suggested in the previous works [35, 36]. Note that the scales of vertical axes are different for the three nuclei.

TABLE I. Binding energies (in MeV) for ^{4}He, ^{16}O and ^{40}Ca, calculated by BHF and RBHF with the $V_{\text{low-}k}$ Argonne v_{18} potential [12], compared with other *ab-initio* calculations with the same effective potential. We take Λ=1.9 fm^{-1} for ^{4}He, and Λ = 2.1 fm^{-1} for ^{16}O and ^{40}Ca as in Refs. [35, 36]. N_{shell}=12, $\hbar\Omega$ = 14 MeV are taken for ^{4}He, and N_{shell}=12, $\hbar\Omega$ = 22 MeV for ^{16}O and ^{40}Ca.

	^{4}He	^{16}O	^{40}Ca
BHF	−25.90	−134.16	−552.14
RBHF	−25.90	−134.15	−549.79
Exact (FY [34, 35])	−29.19(5)	–	–
IT-NCSM [36]	–	−138.0	−462.7
CCSD [35]	−28.9	−142.8	−491.2
CCSD(T) [35]	−29.2	−148.2	−502.9
HF-MBPT(3) [30]	−29.33	−159.34	−600.08
Experiment [37]	−28.30	−127.62	−342.05

with N_{shell}=12. The RBHF gives similar binding energies to the BHF calculations for ^{4}He and ^{16}O, and less energy (by about 2 MeV) for ^{40}Ca.

Table I shows quantitative comparisons with the benchmarks given by other *ab initio* calculations. Nogga *et al,* [34] first calculated the ^{4}He ground-state energy by solving the FY equations with the two-body $V_{\text{low-}k}$. They estimated an accuracy of 50 keV for the calculations of the ^{4}He binding energy. The FY results can be considered as the exact solution for benchmarking other calculations. Roth and Navrátil did the IT-NCSM calculations for ^{16}O and ^{40}Ca [36]. They obtained a ground-state energy of −137.7 MeV and a point-nucleon root-mean-square (rms) radius of 2.03 fm for ^{16}O with $N_{\max}$=14 and $\hbar\Omega$=22 MeV. $N_{\max}$ indicates the maximum shell excitation number in model configurations, which defines the truncation of the model space [36]. An exponential extrapolation of the energy gave $E_{N_{\max}\to\infty} = -138.0$ MeV for ^{16}O. For ^{40}Ca with $N_{\max}$=16 and $\hbar\Omega$=24 MeV, a ground-state energy of −461.8 MeV and a point-nucleon rms radius of 2.27 fm were obtained [36]. An exponential extrapolation yielded $E_\infty = -462.7$ MeV. The CCSD and CCSD(T) ground-state energies given in Table I are the results with the extrapolation to infinite model space [35].

Figure 6 shows the ^{4}He, ^{16}O and ^{40}Ca point-nucleon rms radii calculated by BHF and

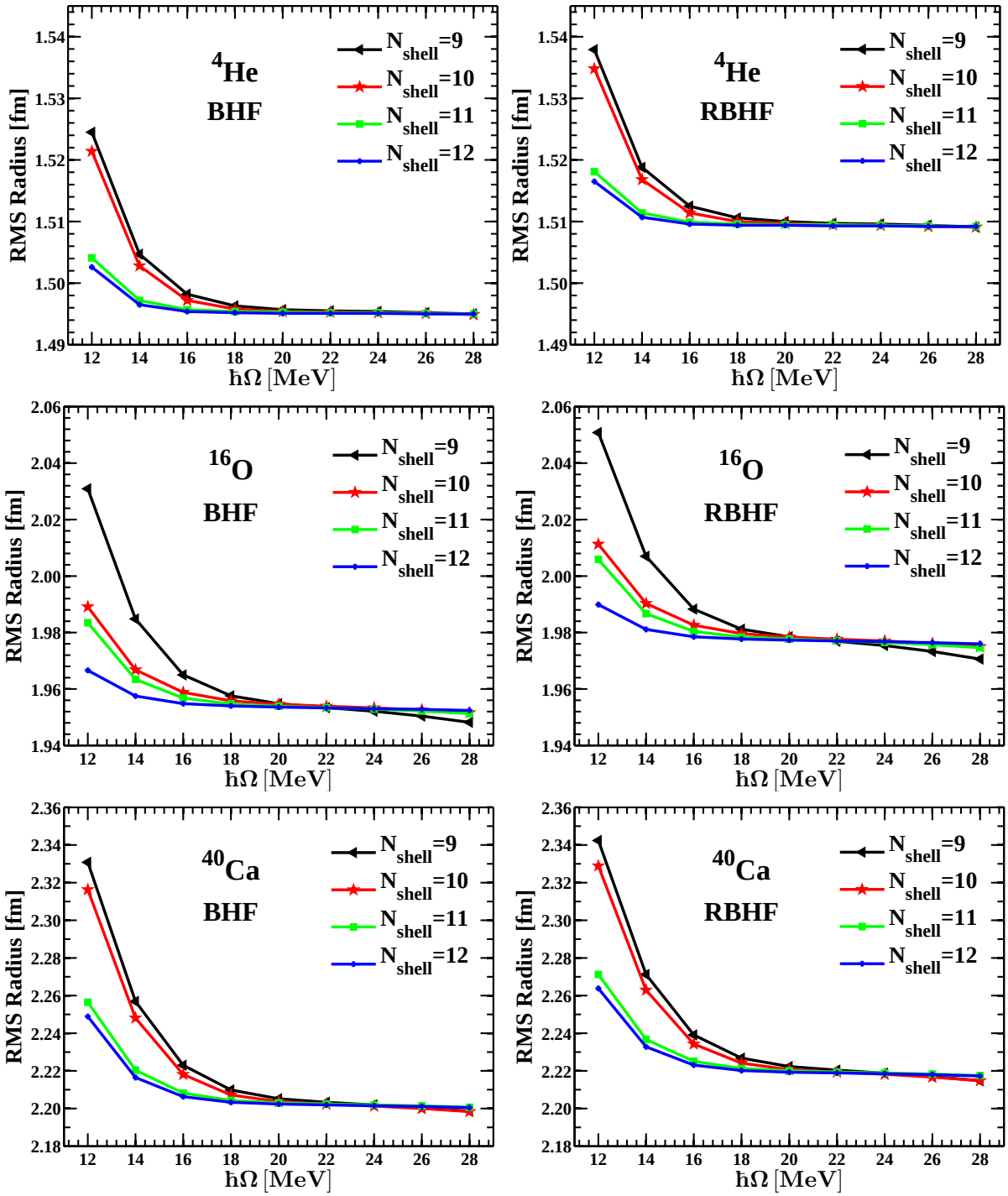

FIG. 6. Similar to Figure 5, but for point-nucleon rms radii.

RBHF as a function of the oscillator parameter $\hbar\Omega$ with different $N_{\rm shell}$. The convergences are similar to the energy calculations. Table II lists the converged results of the point-nucleon rms radii, compared with the IT-NCSM. We see that the RBHF radii are slightly

TABLE II. Calculated point-nucleon rms radii (in fm). The IT-NCSM results are taken from Ref. [36]. The effective interaction, oscillator parameter and $N_{\rm shell}$ (or $N_{\rm max}$) are same as in Table I.

Nuclei	BHF	RBHF	IT-NCSM
^{4}He	1.50	1.51	–
^{16}O	1.95	1.98	2.03
^{40}Ca	2.20	2.22	2.27

larger than the BHF results. The RBHF approach takes into account the depletions of the HF occupied single-particle states due to many-body correlations. When the occupation probability P_h in Eq. (11) gets into the BHF potential U, the single-particle potential is less attractive, and the occupied single-particle levels move up. The interaction of Eq. (9) shows that the RBHF gives smaller kinetic energy and smaller Fermi gap than the BHF calculations. The radius of the nucleus becomes larger when the kinetic energy is reduced [38].

It has been demonstrated [41, 42] that in RBHF the single-particle energies are approximately equal to separation energies, but it does not hold really in BHF. Therefore, in RBHF the single-particle energies can be directly related to experimental removal energies [43, 44]. Experimental single-particle energies are obtained in knockout, stripping and pickup reactions, primarily for the single-particle states close to the Fermi level. Tables III and IV give calculated single-particle energies. We see that RBHF improves slightly the single-particle energies, compared to data. The present calculations do not include three-body and higher-order forces which might have effects on single-particle energies.

The calculated energy differences between the proton and neutron levels are rather small using the Argonne v_{18} potential. For an understanding, we have performed similar BHF and RBHF calculations for ^{16}O using the CD-Bonn potential [10] with the same parameters of $\Lambda = 2.1$ fm^{-1}, $N_{\rm shell} = 12$ and $\hbar\Omega = 22$ MeV. We see that, given in Table V, the CD-Bonn potential with the proton-proton Coulomb interaction leads to clear differences between single-proton and single-neutron energies. However, the ^{16}O binding energy calculated with the CD-Bonn potential is very close to that by the Argonne v_{18} potential. The CD-Bonn potential gives the ^{16}O binding energy of -134.07 MeV in BHF and -133.97 MeV in RBHF, while it is -134.16 MeV and -134.15 MeV in the Argonne v_{18} BHF and RBHF calcula-

TABLE III. Calculated single-particle energies ε (in MeV) for ^{16}O. For orbits below the Fermi surface, occupation probabilities P are modified in the RBHF calculation. Λ=2.1 fm^{-1}, $N_{\rm shell} = 12$ and $\hbar\Omega = 22$ MeV are taken, same as in Table I. The experimental data are taken from Refs. [39, 40].

		^{16}O					
		Neutron			Proton		
Orbits		BHF	RBHF	Expt.	BHF	RBHF	Expt.
$0s_{1/2}$	ε	-73.02	-69.61	-47	-72.75	-69.36	-44 ± 7
	P	1.00	0.98		1.00	0.98	
$0p_{3/2}$	ε	-37.38	-34.87	-21.839	-37.15	-34.65	-18.451
	P	1.00	0.97		1.00	0.97	
$0p_{1/2}$	ε	-24.35	-22.870	-15.663	-24.16	-22.69	-12.127
	P	1.00	0.96		1.00	0.96	
$0d_{5/2}$	ε	-4.65	-3.40	-4.144	-4.49	-3.26	-0.601
$1s_{1/2}$	ε	-2.46	-1.91	-3.273	-2.34	-1.81	-0.106
$0d_{3/2}$	ε	6.84	6.95	0.941	6.90	7.01	4.399

tions, respectively. We note that, in the Argonne v_{18} potential, besides the proton-proton Coulomb interaction there are the proton-neutron Coulomb interaction attributable to the neutron charge distribution, and the proton-neutron and neutron-neutron electro-magnetic interactions via nucleon magnetic moments [12]. The factors might reduce the difference between protons and neutrons.

Table VI gives the calculations with the $V_{\text{low-}k}$ Argonne v_{18} potential at different cutoffs for the nucleus ^{16}O. The results are sensitive to the momentum cutoff of the potential. However, it seems understandable. In a too soft potential with a small cutoff (e.g., $\Lambda = 1.5$ fm^{-1}), induced many-body forces (e.g., three-body force) are significant, implying that one should take into account contributions from the many-body forces. In a hard cutoff (e.g., $\Lambda = 3.0$ fm^{-1}) , high-order correlations beyond HF may need to be considered [30] and a larger model space is required. It has been tested that $\Lambda = 2.1$ fm^{-1} is a suitable cutoff for calculations with the $V_{\text{low-}k}$ potential, which gives weak induced three-body force and weak

TABLE IV. Similar to Table III, but for ^{40}Ca.

		^{40}Ca					
		Neutron			Proton		
Orbital		BHF	RBHF	Expt.	BHF	RBHF	Expt.
$0s_{1/2}$	ε	-137.71	-133.94	–	-137.14	-133.38	-49.1 ± 12
							-77 ± 14
	P	1.00	0.99		1.00	0.99	
$0p_{3/2}$	ε	-92.34	-88.94	–	-91.84	-88.46	-33.3 ± 6.5
	P	1.00	0.99		1.00	0.99	
$0p_{1/2}$	ε	-74.62	-72.21	–	-74.16	-71.77	-32 ± 4
	P	1.00	0.99		1.00	0.99	
$0d_{5/2}$	ε	-53.13	-50.24	-21.30	-52.70	-49.82	-14.9 ± 2.5
							-13.8 ± 7.5
	P	1.00	0.98		1.00	0.98	
$1s_{1/2}$	ε	-43.33	-41.06	-18.104	-42.88	-40.64	-10.850
	P	1.00	0.97		1.00	0.97	
$0d_{3/2}$	ε	-28.15	-26.38	-15.635	-27.80	-26.04	-8.328
	P	1.00	0.95		1.00	0.95	
$0f_{7/2}$	ε	-16.21	-14.20	-8.363	-15.88	-13.88	-1.085
$1p_{3/2}$	ε	-10.45	-9.27	-6.420	-10.16	-9.00	0.631
$1p_{1/2}$	ε	-3.06	-2.40	–	-2.85	-2.21	–
$0f_{5/2}$	ε	8.26	8.55	–	8.40	8.69	–

high-order correlations but good convergence [35, 36].

Besides the matrix inversion method, there is another approximating method to solve the G-matrix elements in Eq. (7), that is iteration [45, 46]. In the iteration approximation, the G-matrix operator of Eq. (2) is expressed as a sum of terms

$$G(\omega) = V + V\frac{Q}{e}V + V\frac{Q}{e}V\frac{Q}{e}V + \dots . \tag{16}$$

It has been proved that the convergence of the iteration is rapid [45, 46]. Usually, the expansion of Eq. (16) up to the third term can give well converged results [45]. In Table VII,

TABLE V. Similar to Table III, but the $V_{\text{low-}k}$ effective interaction is derived from the CD-Bonn potential [10].

		^{16}O					
		Neutron			Proton		
Orbits		BHF	RBHF	Expt.	BHF	RBHF	Expt.
$0s_{1/2}$	ε	-78.89	-76.14	-47	-73.92	-71.34	-44 ± 7
	P	1.00	0.99		1.00	0.99	
$0p_{3/2}$	ε	-40.60	-38.51	-21.839	-35.81	-33.87	-18.451
	P	1.00	0.98		1.00	0.98	
$0p_{1/2}$	ε	-25.98	-24.72	-15.663	-21.35	-20.25	-12.127
	P	1.00	0.96		1.00	0.96	
$0d_{5/2}$	ε	-5.97	-4.90	-4.144	-1.37	-0.47	-0.601
$1s_{1/2}$	ε	-3.31	-2.82	-3.273	0.70	1.03	-0.106
$0d_{3/2}$	ε	6.90	7.00	0.941	10.37	10.38	4.399

TABLE VI. Single-proton energies (ε_i), occupation probabilities (P_i), binding energies and the point-nucleon rms radii $\langle r \rangle$ in ^{16}O, calculated with different $V_{\text{low-}k}$ cutoffs. $N_{\text{shell}} = 12$ and $\hbar\Omega = 22$ MeV are taken. All energies are given in MeV and radii in fm. Single-neutron states have similar behaviors to single-proton orbits with increasing Λ value.

	Λ=1.5 fm^{-1}		Λ=2.1 fm^{-1}		Λ=3.0 fm^{-1}	
	BHF	RBHF	BHF	RBHF	BHF	RBHF
$\varepsilon_{s_{1/2}}$	-84.23	-83.27	-72.75	-69.36	-45.84	-41.12
$\varepsilon_{p_{3/2}}$	-42.09	-41.40	-37.15	-34.65	-21.89	-18.77
$\varepsilon_{p_{1/2}}$	-32.03	-31.49	-24.16	-22.69	-15.92	-13.83
$P_{s_{1/2}}$	1.00	0.997	1.00	0.982	1.00	0.949
$P_{p_{3/2}}$	1.00	0.991	1.00	0.972	1.00	0.947
$P_{p_{1/2}}$	1.00	0.996	1.00	0.957	1.00	0.936
E	-194.39	-194.36	-134.16	-134.15	-64.20	-64.38
$\langle r \rangle$	1.95	1.96	1.95	1.98	2.32	2.40

TABLE VII. The BHF and RBHF calculations of binding energies (in MeV) with different prescriptions, see the corresponding text for the details of the different prescriptions. The effective interaction, $N_{\rm shell}$ and $\hbar\Omega$ are same as in Table I.

Nuclei		G-inversion	G-iteration	U-approximation
^{4}He	BHF	-25.90	-25.83	-25.06
	RBHF	-25.90	-25.83	-25.31
^{16}O	BHF	-134.16	-134.07	-125.39
	RBHF	-134.15	-134.07	-128.08
^{40}Ca	BHF	-552.14	-552.16	-529.02
	RBHF	-549.79	-549.85	-535.10

we list the results of the G-iteration method, compared with the G-inversion calculations. In the G-iteration calculations, we consider only the first three terms of Eq. (16), and obtain the well converged binding energies for both BHF and RBHF calculations. The numerical solution of the G-iteration approximation is less complicated, compared with the G-inversion method. From the calculations, we see indeed that the iterative solution of the Bethe-Goldstone equation (i.e., Eq. (2)) converges rapidly, and the matrix inversion method gives the stable solutions of the equation.

As another approximation for the BHF potential U in Eq. (5), Refs. [1, 5, 26] assumed the particle-particle elements $\langle a|U|b\rangle = 0$ for $a, b > \varepsilon_{\rm F}$, which we call U-approximation in this paper. With the U-approximation, we have performed the BHF and RBHF calculations with the G-matrix elements solved by the inversion method. In Table VII, we see that the U-approximation brings some changes in the calculated binding energies. However, the changes in the RBHF calculations are less than in the BHF calculations. This implies the self-consistent occupation probabilities can suppress the effect from the different choices of the potential U. In RBHF, the influence from the uncertainty of the particle-particle elements $\langle p_1|U|p_2\rangle$ can be partially compensated by occupation probabilities.

IV. SUMMARY

We have performed the BHF and RBHF calculations for finite nuclei with the $V_{\text{low-}k}$ renormalized NN interaction. The G-matrix and associated Pauli exclusion operator are treated in the BHF or RBHF basis, giving self-consistent descriptions. The RBHF which is renormalized with single-particle occupation probabilities resulting from many-body correlations gives improved single-particle energies and nuclear radii. Different techniques are taken to solve the Bethe-Goldstone equation. The iteration of the Bethe-Goldstone equation converges rapidly, while the inversion method gives stable solution. The evaluations of particle-particle matrix elements of the BHF potential are somewhat controversial because their diagrams require off-shell definitions regarding the starting energy. Different prescriptions for the particle-particle matrix elements have been tested in the present calculations. We find that even if the particle-particle matrix elements are set to be zero, the final results of the BHF and RBHF calculations do not change significantly.

The calculations are limited to closed-shell spherical nuclei, and the angular momentum coupling scheme has been employed. The doubly magic nuclei, ^{4}He, ^{16}O and ^{40}Ca, were well calculated. The convergences with respect to the HO frequency and model truncation are have been analyzed in detail. The general results are consistent with other *ab initio* methods (Faddeev-Yakubovsky solution, no-core shell model, coupled cluster and many-body perturbation theory). Three-body forces which are not included should improve the calculations.

ACKNOWLEDGMENTS

Valuable discussions with J. P. Vary, H. Müther, L. Coraggio and J. C. Pei are gratefully acknowledged. This work has been supported by the National Key Basic Research Program of China under Grant No. 2013CB834402; the National Natural Science Foundation of China under Grants No. 11235001, No. 11320101004 and NO. 11575007; the CUSTIPEN (China-U.S. Theory Institute for Physics with Exotic Nuclei) funded by the U.S. Department of

Energy, Office of Science under grant number DE-SC0009971.

[1] P. Ring and P. Schuck, *The nuclear many-body problem* (Springer-Verlag, 1980).

[2] L. Coraggio, N. Itaco, A. Covello, A. Gargano, and T. T. S. Kuo, Phys. Rev. C **68**, 034320 (2003).

[3] M. A. Hasan, J. P. Vary, and P. Navrátil, Phys. Rev. C **69**, 034332 (2004).

[4] R. Roth, P. Papakonstantinou, N. Paar, H. Hergert, T. Neff, and H. Feldmeier, Phys. Rev. C **73**, 044312 (2006).

[5] H. Müther and P. U. Sauer, *Computational Nuclear Physics 2*, edited by K. Langanke, J. A. Maruhn, and S. E. Koonin (Springer-Verlag New York, 1993) p. 30.

[6] K. T. R. Davies and R. J. McCarthy, Phys. Rev. C **4**, 81 (1971).

[7] R. L. Becker, Phys. Rev. Lett. **24**, 400 (1970).

[8] R. L. Becker, K. T. R. Davies, and M. R. Patterson, Phys. Rev. C **9**, 1221 (1974).

[9] A. H. Lippok and H. Müther, Phys. Rev. C **92**, 034312 (2015).

[10] R. Machleidt, Phys. Rev. C **63**, 024001 (2001).

[11] V. G. J. Stoks, R. A. M. Klomp, C. P. F. Terheggen, and J. J. de Swart, Phys. Rev. C **49**, 2950 (1994).

[12] R. B. Wiringa, V. G. J. Stoks, and R. Schiavilla, Phys. Rev. C **51**, 38 (1995).

[13] P. Doleschall, Phys. Rev. C **69**, 054001 (2004).

[14] D. R. Entem and R. Machleidt, Phys. Rev. C **68**, 041001 (2003).

[15] R. Machleidt and D. Entem, Physics Reports **503**, 1 (2011).

[16] K. A. Brueckner, Phys. Rev. **97**, 1353 (1955).

[17] J. Goldstone, Proceedings of the Royal Society of London. Series A, Mathematical and Physical Sciences **239**, pp. 267 (1957).

[18] H. A. Bethe, B. H. Brandow, and A. G. Petschek, Phys. Rev. **129**, 225 (1963).

[19] M. Hjorth-Jensen, T. T. Kuo, and E. Osnes, Physics Reports **261**, 125 (1995).

[20] P. U. Sauer, Nuclear Physics A **150**, 467 (1970).

[21] R. J. Eden and V. J. Emery, Proceedings of the Royal Society of London. Series A, Mathematical and Physical Sciences **248**, pp. 266 (1958).

[22] S. Bogner, T. T. S. Kuo, L. Coraggio, A. Covello, and N. Itaco, Phys. Rev. C **65**, 051301

(2002).

[23] S. Bogner, T. Kuo, and A. Schwenk, Physics Reports **386**, 1 (2003).

[24] J. Kuckei, F. Montani, H. Müther, and A. Sedrakian, Nuclear Physics A **723**, 32 (2003).

[25] G. Hagen, M. Hjorth-Jensen, and N. Michel, Phys. Rev. C **73**, 064307 (2006).

[26] I. S. Towner, *A shell model description of light nuclei* (Clarendon Press Oxford, 1977) p. 61.

[27] I. Shavitt and R. J. Bartlett, *Many-Body Methods in Chemistry and Physics: MBPT and Coupled-Cluster Theory* (Cambridge University Press, 2009).

[28] K. T. R. Davies, M. Baranger, R. M. Tarbutton, and T. T. S. Kuo, Phys. Rev. **177**, 1519 (1969).

[29] R. Rajaraman and H. A. Bethe, Rev. Mod. Phys. **39**, 745 (1967).

[30] B. S. Hu, F. R. Xu, Z. H. Sun, J. P. Vary, and T. Li, Phys. Rev. C **94**, 014303 (2016).

[31] R. J. McCarthy and K. T. R. Davies, Phys. Rev. C **1**, 1644 (1970).

[32] B. H. Brandow, Phys. Rev. **152**, 863 (1966).

[33] B. H. Brandow, Rev. Mod. Phys. **39**, 771 (1967).

[34] A. Nogga, S. K. Bogner, and A. Schwenk, Phys. Rev. C **70**, 061002 (2004).

[35] G. Hagen, D. J. Dean, M. Hjorth-Jensen, T. Papenbrock, and A. Schwenk, Phys. Rev. C **76**, 044305 (2007).

[36] R. Roth and P. Navrátil, Phys. Rev. Lett. **99**, 092501 (2007).

[37] G. Audi, F. Kondev, M. Wang, B. Pfeiffer, X. Sun, J. Blachot, and M. MacCormick, Chinese Physics C **36**, 1157 (2012).

[38] H. Müther, R. Machleidt, and R. Brockmann, Phys. Rev. C **42**, 1981 (1990).

[39] Data extracted using the NNDC On-Line Data Service, http://www.nndc.bnl.gov/.

[40] M. A. K. Lodhi and B. T. Waak, Phys. Rev. Lett. **33**, 431 (1974).

[41] R. L. Becker and M. R. Patterson, Nuclear Physics A **178**, 88 (1971).

[42] T. Koopmans, Physica **1**, 104 (1934).

[43] G. J. Wagner, "Single-nucleon removal energies," in *Nuclear Structure Physics: Proceedings of the Minerva Symposium on Physics held at the Weizmann Institute of Science Rehovot, April 2–5, 1973*, edited by U. Smilansky, I. Talmi, and H. A. Weidenmüller (Springer Berlin Heidelberg, Berlin, Heidelberg, 1973) pp. 16–57.

[44] A. E. L. Dieperink and T. de Forest Jr., Annual Review of Nuclear Science **25**, 1 (1975).

[45] R. K. Tripathi, A. Faessler, and H. Müther, Phys. Rev. C **10**, 2080 (1974).

[46] M. R. Anastasio, A. Faessler, H. Müther, K. Holinde, and R. Machleidt, Phys. Rev. C **18**, 2416 (1978).